Improved spatio-temporal measurements of visually evoked fields using optically-pumped magnetometers

Aikaterini Gialopsou[1,2,*], Christopher Abel[1], Timothy M. James[1], Thomas Coussens[1], Mark G. Bason[1], Reuben Puddy[1], Francesco Di Lorenzo[2], Katharina Rolfs[3], Jens Voigt[3], Tilmann Sander[3], Mara Cercignani[2], Peter Krüger[1]

[1] Department of Physics and Astronomy, University of Sussex, Falmer, Brighton BN1 9HQ, United Kingdom
[2] Clinical Imaging Sciences Centre, University of Sussex, Falmer, Brighton BN1 9PH, United Kingdom
[3] Physikalisch Technische Bundesanstalt, D-10587 Berlin, Germany

*a.gialopsou@sussex.ac.uk

Recent developments in performance and practicality of optically pumped magnetometers have enabled new capabilities in non-invasive brain function mapping through magnetoencephalography (MEG). In particular the lack of need of cryogenic operating conditions allows for more flexible placement of the sensor heads closer to the brain surface, leading to improved spatial measurement resolution and increased source localisation capabilities. Through recordings of visually evoked brain fields (VEF) we demonstrate that the greater sensor proximity can be further exploited to improve the temporal resolution. We use an OPM and for reference a superconducting quantum interference device (SQUID) setup to measure brain responses to standard flash and pattern reversal stimuli. We find highly reproducible signals with consistency across multiple healthy participants, stimulus paradigms and sensor modalities. The temporal resolution advantage of OPMs is manifest in a fourfold enhanced ratio of magnetic signal peak height to temporal width as compared to SQUIDs. The resulting capability of improved spatio-temporal signal tracing is illustrated by simultaneous vector recordings of VEFs in the V1 and V2 areas of the visual cortex, where a time lag on the order of 10-20 ms is consistently found. This paves the way for further studies of spatio-temporal neurophysiological signal tracking in visual stimulus processing and other brain responses with potentially far-reaching consequences for time-critical mapping of functionality in the healthy and pathological brain.
Keywords : MEG, optically-pumped magnetometer, OPM-MEG, SQUID-MEG, spatio-temporal resolution

1 Introduction

Over the last century, outstanding advances in medical physics have led to the development of non-invasive functional neuroimaging techniques [1–3]. This has provided significant insights into brain function and connectivity. An important ingredient is that modern neuroimaging techniques allow the neural patterns associated with specific stimulations to be investigated [4], providing information about the signal's spatial and temporal characteristics [5]. Previous studies have shown that spatio-temporal analysis of brain signals is not only essential to understand the basic mechanisms of brain circuits, but would also provide reliable biomarkers for differentiating physiological and pathological brain activity in neurodegenerative diseases [6,7]. There is even a potential for predicting clinical progression or treatment responses [8]. The realisation of the full scope of temporal and spatial localisation of brain signals, however, is hampered by the intrinsically low spatio-temporal resolution of currently available methods [9, 10].

Established neuroimaging techniques are limited in either temporal or spatial resolutions, which makes identification of propagating signals challenging. Functional Magnetic Resonance Imaging is capable of mapping activated brain regions with high spatial and low temporal resolutions ($> 1\,$s), as the local measured changes in blood flow are not synchronized with neuronal activity [11]. Electroencephalography (EEG) is a real-time neuroimaging method, with limited source localisation capability and spatial resolution ($\sim 10\,$mm) [12].

Magnetoencephalography (MEG) is an alternative real-time method with a theoretically possible improved spatial resolution, able to measure postsynaptic potentials of tangential pyramidal cells at the surface of the scalp [12]. Recent research has shown that MEG can be used for the evaluation of abnormal cortical signals in patients with Alzheimer's disease [13], Parkinson's disease [14], autism spectrum disorder [15], and in severe cases of post-traumatic stress disorder [16]. However, MEG suffers from low signal-to-noise ratio (SnR), and its use is confined to magnetically-shielded rooms (MSR). The magnetically shielded environments are used to subdue environmental magnetic noise, often many orders of magnitude higher than neuromagnetic fields ($\sim 10^{-15}\,$T).

Traditionally, MEG relies on an array of superconductive quantum interference devices (SQUIDs) to measure the brain's magnetic fields [17]. With the sensor array being fixed inside the required cryogenic dewar, the locations of the individual sensors must be arranged to

fit a vast majority of head sizes and shapes [18]. The fixed positions result in different radial offsets from a subject's head; coupled with tiny head movements from a subject during a measurement, both have a major impact on the potential cortical activity detection [19]. In particular, the theoretically achievable precision of signal source localisation is lost. This makes SQUID-MEG impractical in many cases, in particular in the clinical context.

Extremely sensitive spin-exchange relaxation free (SERF) optically-pumped magnetometers (OPMs), developed at the turn of the millennium [20], can help to overcome the drawback of limited spatial resolution of SQUID-MEG [21]. With the sensors being fixed to a subject's head [22], a smaller offset distance than SQUIDS, and the ability for simultaneous dual axis measurements, OPM-MEG has several advantages over SQUID-MEG, including its suitability for applications within pediatric and clinical populations.

The aim of this study is to demonstrate the improved ability of OPM-MEG to record spatio-temporal characteristics of neurophysiological signals in comparison to conventional SQUID-MEG. As a prototypical test case we have chosen the visual cortex response to established standard visual stimulations, so that the measured responses can be evaluated in a well-characterised context. We find that OPM-MEG is superior to SQUID-OPM in brain signal tracking in space and time and is thus a suitable method to provide new information about propagating signals, source localisation, the neural speed, and the brain circuits far beyond the processing of visual stimuli.

2 THEORY CONSIDERATIONS

2.1 Spatial resolution

The fact that magnetic fields decay according to a power law with the distance from a field source is the reason for improved signal detection when sensors are moved closer to the brain. As shown formally for a generic situation [23] and confirmed through realistic brain anatomy simulations [24, 25], the consequences of the field decay law are that closer positioning of a sensor system provides improved signal-to-noise, better spatial resolution and more precise source localisation. In general, when applying the Rayleigh criterion for resolution, the maximum distance at which two sources can be resolved is comparable to the distance between the two sources [23]. As OPMs can be placed closer to the head than SQUID systems, the OPMs are able to achieve a higher spatial resolution.

2.2 Vectoral measurements

In conventional MEG only one component of the vectorial magnetic field is measured. Most commercial setups for SQUID-MEG only measure magnetic field gradients radial to the brain. This is because at the typical stand-off distances of several centimetres the orthogonal components tend to be weak, so that the radial field (gradient) component approximates the total field (gradient) magnitude well. For closer proximity of the sensors to the brain, as enabled by OPMs, measuring multiple field (gradient) components rather than just signal strengths results in an ability to extract extra spatial information [26]. A vector rather than scalar measurement taken at short distances does not suffer from the zone of a vanishing field component in the immediate vicinity of a current dipole and is sensitive to volume currents in the brain.

Measuring both radial and tangential field components also helps to improve signal *temporal* resolution. This is a consequence of the ability to characterise the field as a vector. At the sensor, the magnetic field has a direction and magnitude. A radial sensor measures the magnetic field projected onto the radial direction. By measuring in only the radial direction it is not possible to differentiate the difference between a rotation or a change in magnitude of the magnetic field vector. Worse still, if the magnetic field vector simultaneously changes in both direction and magnitude, then the time at which the magnetic field reaches peak magnitude can be obscured. By measuring a second component of the magnetic field we can begin to differentiate between a change in the magnitude of the magnetic field and a change in magnetic field direction. Sensors near the head are in a source-free region, therefore using Ampère's Law $\nabla \times B = 0$ the third magnetic field component can be calculated from the other two magnetic field components assuming the gradient of the magnetic field can be calculated. For a system with a low sensor count, all three magnetic field components need to be measured to achieve a full determination of the magnetic field.

3 MATERIALS AND METHODS

3.1 Participants and MRI

Visual evoked fields were studied in 3 healthy participants (2 men aged 26 and 30, 1 woman aged 47 years), with normal or corrected-to-normal vision. The 3 participants received a 3 T MRI scan at the University of Sussex (UK), including a high-resolution T1-weighted anatomical scan. For one participant a diffusion-weighted scan was acquired with the purpose of reconstructing the optic radiations. The acquisition had 2 diffusion-weighting shells (b values = 1000 and 3000 smm^{-2}). For each b value, diffusion gradients were ap-

plied along 60 non-collinear directions. Six images with no diffusion weighting (b=0) were also collected. Image processing was done using tools from the FMRIB's Diffusion Toolbox 5.0. First, data were corrected for involuntary motion and eddy currents using affine registration. Next, BEDPOSTx was run with default settings to fit a crossing fibers model [27]. Finally, XTRACT was used to automatically reconstruct the left and right optic radiations in native space by probabilistic tractography [28]. The results are shown in Figure 1.

3.2 Experimental Design

The study was approved by the Brighton and Sussex Medical School Research Governance and Ethics Committee (ER/BSMS3100/1), and all participants gave written informed consent to take part, after explanation of the procedure and purpose of the experiment. All MEG measurements were taken in the Ak3b MSR (Vacuumschmelze, Hanau, Germany) at Physikalisch-Technische Bundesanstalt (PTB), Berlin . This MSR is equipped with a triaxial active shielding coil system on the outside controlled by fluxgates. Inside the MSR field fluctuations are sufficiently weak to allow OPM operation [29], [30].

Two standard full-field visual stimulation protocols were employed during the MEG recording, a flash stimulus (FS), and a pattern reversal stimulus (PR). The parameters used were based on standard guidelines for clinically evoked potentials [31]. These paradigms are widely used to evaluate early visual processing, and to detect abnormalities in the visual pathways. The flash stimulus, shown in figure 1(a), consisted of short white flashes of length 0.08 s (5 frames). To avoid participants from preempting the stimulus, each white flash was followed by a dark period with the length varying pseudo-randomly between 0.92 s and 1.00 s (55 to 60 frames). The total duration of a single FS measurement run was 300 s.

The pattern-reversal stimulus, figure 1(b), consisted of a black and white checkerboard (10 squares wide, 8 high) with the colours inverting at 0.5 s (30 frame) intervals. Each run had a duration of 280 s. For both FS and PR, a red dot was continuously projected onto the centre of the screen to act as a focal point for the participant. Before each measurement run, whilst in position for the trial, the participants were exposed to a three-minute dark adaptation period. Measurements of the empty MSR were obtained in order to evaluate environmental noise levels. During the noise measurements, the OPMs were located in the same position and orientation as they would with a participant wearing the sensors. For the OPM-MEG, participants sat upright with the sensors mounted in a 3D-printed helmet (figure 1(c)). A chin rest was used to help stabilise each subject's head, reducing movement when looking forward at a $50\times34\,\mathrm{cm}^2$ vertically orientated screen. The stimuli were projected on to the screen via a mirror system from a 60 Hz LCD projector, positioned outside of the MSR. The SQUID-MEG system (figure 1(e)) accommodated participants in a horizontal position, with the same screen then positioned horizontally above the subject. The screen to eye distance was 53 cm for the OPM-MEG setup and 45 cm for the SQUID-MEG system.

4 MEG SYSTEMS OVERVIEW

4.1 OPM-MEG

The OPM-MEG system consisted of two second-generation QuSpin zero-field magnetometers (QuSpin Inc., Louisville, CO, USA), with a specified typical sensitivity $\lesssim 15\,\mathrm{fT/Hz^{1/2}}$ and magnetic field measurement bandwidth of 135 Hz in a $12.4\times16.6\times24.4\,\mathrm{mm^3}$ package (sensor head). The OPMs were mounted in a 3D printed helmet (open-source design; OpenBCI Mark IV helmet) [1] such that they were positioned over the visual cortex at Oz and POz positions, according to the standard 10-20 system [32]. These locations were chosen in accordance with the optical radiation pattern findings obtained through MRI (Figure 1) in order to cover different locations where evoked signals could be detected with a potential for differential time lags. The sensors placed at Oz and POz correspond to the primary visual cortex (V1) and the associative visual cortex (V2), respectively. Studies have shown the feed-forward and feedback interaction between the V1 and V2 areas in response to visual stimulation [33]. More particularly, there is an early activation at V1, known as the P1 or C1 component, which is suppressed when the signal propagates to V2, after which a reflected wave is initiated and propagates back to V1 [34].

The scalp to sensor distance was fixed to ~ 5 mm by the design of the helmet and sensor package. Custom-made Python-based software was developed for the design and presentation of stimuli. The software was directly connected and synchronized with the main OPM-MEG data acquisition system (DAQ). The OPM-MEG system's analogue output was recorded at 1 kHz via a Labjack T7 pro (Labjack Corporation, Co, USA). All the DAQ electronics, except the OPM sensor-heads, were located outside the MSR and directly connected to the Labjack and control computer.

4.2 SQUID-MEG

The SQUID-MEG system MEGvision (Yokogawa Electric Corporation, Japan) comprised of 125 axial gradiometers and 3 reference magnetometers. For the stimuli presentation the same custom-written software was used, to prevent any bias in the stimulation delivery.

[1] https://github.com/OpenBCI/Ultracortex/tree/master/Mark_IV/MarkIV-FINAL

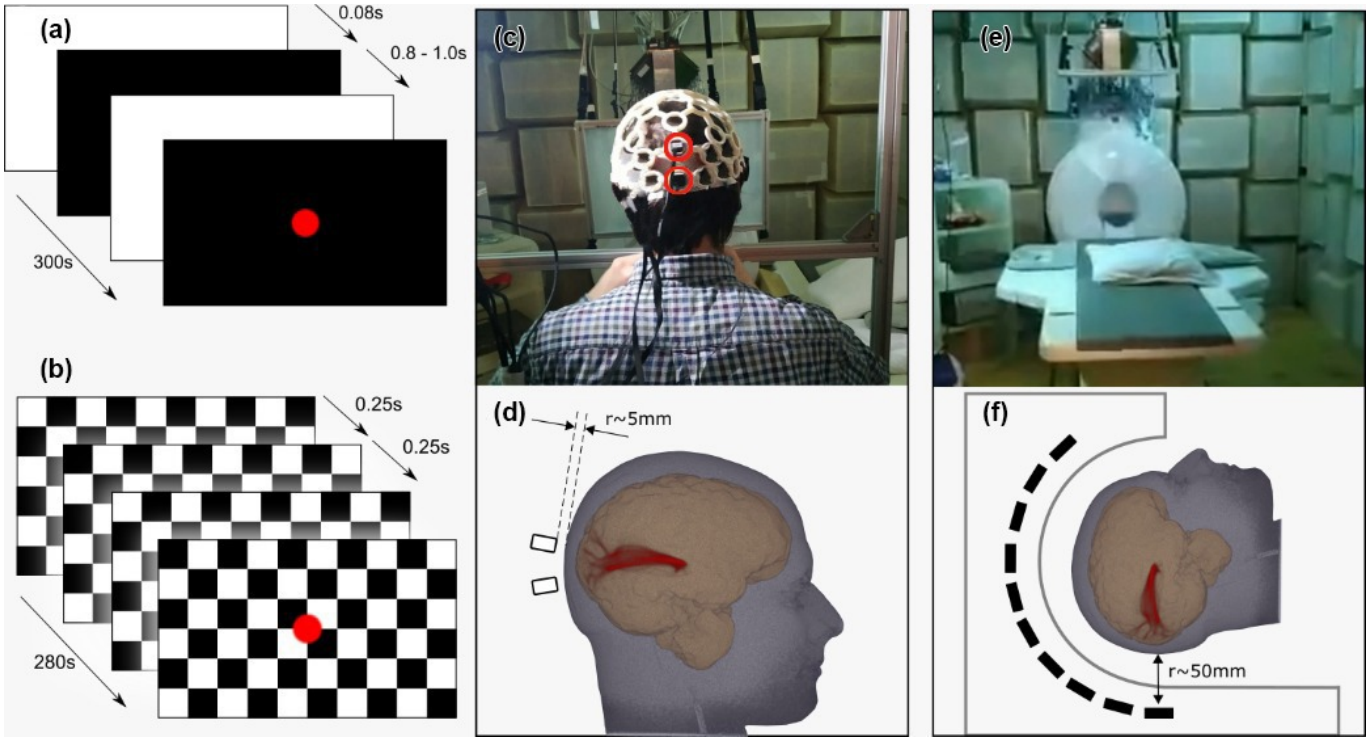

Figure 1: (a) Flash and (b) pattern reversal stimulation protocols. (c) A participant in position with the 3D printed helmet containing the OPM devices. Red highlighted cells show the sensor locations used for the study. (d) 3D rendering of the MRI scan of Participant 1 showing approximate locations of OPM sensors 1 & 2, and scalp-sensor separation of around 5 mm. The reconstructed optic radiation are also shown in red. (e) The Yokogawa SQUID-MEG system. (f) Schematic of the SQUID-MEG system showing a sensor to scalp separation of approximately 50 mm.

Data from all sensors were recorded, and the sensors located closest to the OPM positions were used for analysis. The fixed positions of the sensors resulted in a ~ 50 mm standoff from the subject's scalp. The SQUID-MEG used MEG Laboratory 2.004C (Eagle Technology Corporation) data acquisition software, with a 2 kHz sampling frequency.

4.3 Data Analysis

Both DAQ systems were synchronised with the presentation software. Both OPM and SQUID data analysis was performed using the FieldTrip toolbox [35] and MATLAB. In order to isolate the frequencies of interest with relevance in visually evoked potentials, all data were filtered with a bandpass filter between 5 and 40 Hz. Further bandstop filters were applied between 9 and 11 Hz to remove non physiological artifacts observed in empty MSR measurements, and between 49 and 51 Hz to further suppress 50 Hz line-noise. The epoched trials for FS were -45 ms to 350 ms, and 0 ms to 250 ms for PR. Any trials with interrupted recordings were removed from the analysis. All the time-locked averaged responses contain more than 380 trials for the FS stimulation, and more than 280 for PR.

In the following sections the evoked fields are shown as the mean across all individual trials for a single run. The uncertainties on the signal amplitudes are calculated as the standard error at each time point (with a 1 ms time spacing for OPM-MEG and 0.5 ms for SQUID-MEG). The resulting uncertainty band is then used to determine temporal uncertainties of signal features such as amplitude peaks. The time error is set as the width of the uncertainty band at the amplitude feature.

In order to compare the spatio-temporal response of OPM-MEG to SQUID-MEG we initially study the temporal resolution of the two systems by measuring the signal height to (temporal) width ratio (HWR) in characteristic evoked magnetic field peaks. In each visually evoked fields (VEF) we found the dominant peaks for each sensor type and estimated the HWR. The signal height is taken as the difference between the signal at the peak maximum and the mean of the two adjacent local minima. The width is estimated as the time difference between the two local minima (see insert in Figure 2). The HWR uncertainty results as error propagated from time and signal uncertainties, determined in the above described manner.

In a second step, the evoked potentials as measured at the two sensor locations are then compared. For the OPM system, the simultaneously obtained individual field component (radial B_z and axial B_y) data are further compared to the resulting planar projection B_{yz}, with $|B_{yz}| = \sqrt{B_y^2 + B_z^2}$. This is done to effectively rule out timing artefacts that can occur in data restricted to an individual component.

VEFs are characterized by 3 time components occurring at different times: the early component (P1), the main component (P2 for flash stimuli and P100 for pattern reversal stimuli), and the late component (P3). For the component analysis, we established the onset range for the main and late components (P2/P100, P3) based on previous studies [10,36–40]. The flash and pattern reversal stimulus responses consist of an early component with peak onset between 35 and 60 msec, a main component (P2) between 83 and 152 msec, and a late component (P3) between 160 and 230 msec. Each participant had at least four FS runs and three PR runs with the OPM-MEG system, and a single run for each stimuli with the SQUID-MEG. The averaged responses were determined using the same method as detailed above.

5 RESULTS

The VEFs from all participants and all modalities were consistent with patterns known from the literature (see in Figure 2). Consistency between multiple runs of equal paradigms applied to each participant was high (see Figure 3). To quantify the degree of reproducibility we measured the Pearson correlation coefficient for the Oz sensor between runs for each participant. We found the respective correlation coefficients for the flash stimulus and pattern reversal as 0.83(0.06) and 0.82(0.12), for Participant 1, 0.77(0.12) and 0.24(0.05) for Participant 2 and 0.80(0.07) and 0.46(0.14)for Participant 3.

We consider the height to width ratio (HWR) of the two systems and the higher SnR of OPM-MEG observed in other studies [22, 24]. Figure 2 shows measurements from a single OPM sensor and the corresponding SQUID sensor for FS. The OPM-MEG recorded signals with up to 4 times higher amplitude than the SQUID-MEG, with the OPM and SQUID sensors recording a maximum amplitude of $\sim$450(40) fT and $\sim$113(4) fT, respectively. Along with the increase in amplitude over the SQUIDs, we see the same activation patterns in both methods, further verifying the OPM's recorded traces. The OPM HWR was found to be 12(2) fT/msec, compared to the SQUID HWR of 3.2(0.2) fT/msec. The OPM's higher HWR indicates a higher temporal resolution of the OPM-MEG neuroimaging system. The OPM VEF shows more pronounced peaks, with sharply defined maxima and minima, resulting in a lower uncertainties compared to SQUID-MEG measurements.

In Figure 3 we plot all runs recorded by OPM-MEG, along with their average, for Participant 1. The results are recorded at Oz during FS (a) and PR (b) stimuli. The individual runs show the reproducibility of the activation patterns during both stimulations, with the main (P2 or P100) and late components (P3) having similar time onsets across all runs. For FS, the main component (P2) has an onset time between 90 ms and 100 ms and the late component (P3) between 180 ms and 190 ms. For PR, the main component P100 occurs between 128 ms and 133 ms, while the late component (P3)

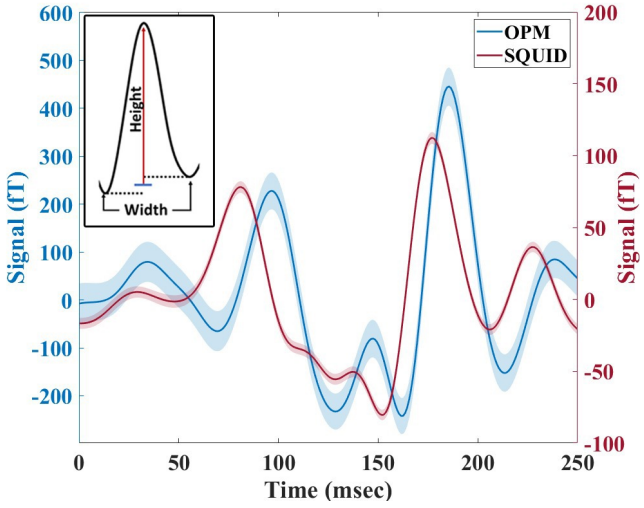

Figure 2: Averaged evoked field recorded by OPM-MEG and SQUID-MEG for Participant 1 for flash stimulation over a single measurment run (300 trials). VEF measured at Oz using OPM sensor (blue line) and the corresponding SQUID sensor (red line).The shaded area shows the standard error. Inset: The signal height (red line) is the amplitude difference between the peak maximum and the mean of the two local minima (blue line). The width is the time difference between the two local minima (dashed lines). The HWR is the ratio of these two values.

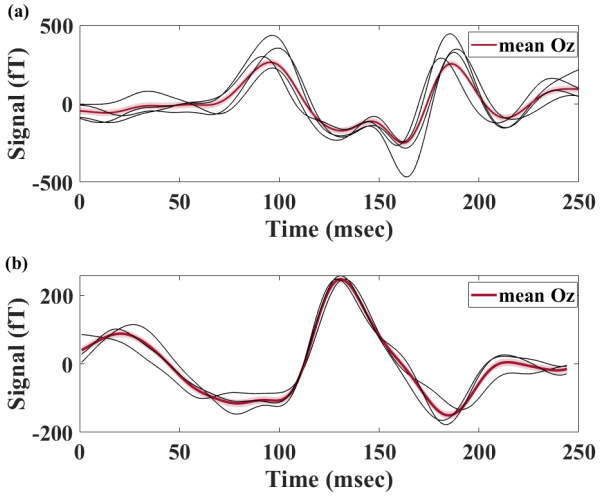

Figure 3: OPM VEF for (a) four flash stimulation runs and the associated mean. (b) Three PR runs along with the mean for Participant 1. The individual runs (black) for both FS and PR show the same activation pattern as the associated mean (red). The shaded area displays the standard error of the mean.

occurs between 210 ms and 214 ms. We confirm the reproducibility across all participants and stimuli.

Figure 4 displays a single run recorded by OPM-MEG (a) and SQUID-MEG (b) systems during FS. The OPM measurements show a significant time difference between the arrival of the signal at POz and Oz for both the main and late components, with an early activation at POz followed by an Oz activation. The vertical purple bands represent the range of P2 and P3 components found in previous studies for Oz EEG sensors [9, 10, 36–40]. The dominant peaks that fall within these boundaries are picked out by bold dashed lines, representing the peak times of the main (P2) and late (P3) components. The times $\Delta\tau_1$ and $\Delta\tau_2$ are defined as the delay between signals arriving at POz and Oz for the main and late components, respectively. For this FS OPM measurement $\Delta\tau_1$ was measured as $\sim$10 (9)ms and $\Delta\tau_2$ as $\sim$18 (4)ms. The earlier activation of POz compared to Oz for Participant 1 was observed in all four runs, with $\overline{\Delta\tau_1}$ = 8(3) ms and $\overline{\Delta\tau_2}$ = 18(1) ms. The reproducibility of the time delay, and the small variations in $\Delta\tau_1$ and $\Delta\tau_2$ over multiple measurement runs point firmly to a neurophysiological origin of the delay, i.e. a recorded true timing difference of signals arriving at different locations within the visual cortex. Simliar time delays are also suggested in Figure 4(b) for the SQUID-MEG measurement, where we find $\Delta\tau_1$ =4(5) ms and $\Delta\tau_2$ = $\sim$18 (4)ms. In spite of the greater signal to noise ratio for SQUID measurements in comparision to our OPM sensor setup, the timing uncertainties for $\Delta\tau_{1,2}$ are similar in both modalities due the improved HWR achieved with OPMs. The observed activation patterns were shown to be reproducible across all runs and stimuli, with activation of POz before Oz being detected in all participants.

While these measurements clearly point to an early activation of the associative visual cortex (POz) followed by the activation of the primary visual cortex (Oz), the unique feature of the OPM sensors of simultaneous measurement along two axes y and z, can be used to further confirm the neurophysiological origin of the delay phenomenon. Figure 5 shows the magnetic field components B_y and B_z simultaneously measured by two OPMs, along with each sensor's magnitude of the yz-plane projection $|B_{yz}|$. In Figure 5(a) we show the OPM-MEG B_y and B_z FS responses recorded simultaneously at POz and Oz. B_z shows a VEF with higher amplitudes and more clearly discernable peak structure than that recorded by B_y. In Figure 5(b) we show $|B_{yz}|$.The characteristic components of the VEF recorded in the vector components persists, including the timings and relative time delays of the main VEF features (previously negative peaks are now positive as the yz-plane projection is displayed as the modulus, which is by defnition non-negative). Our result of a significant and reproducible time delay between signals arriving at POz and Oz (Figures 4 and 5) is consistently

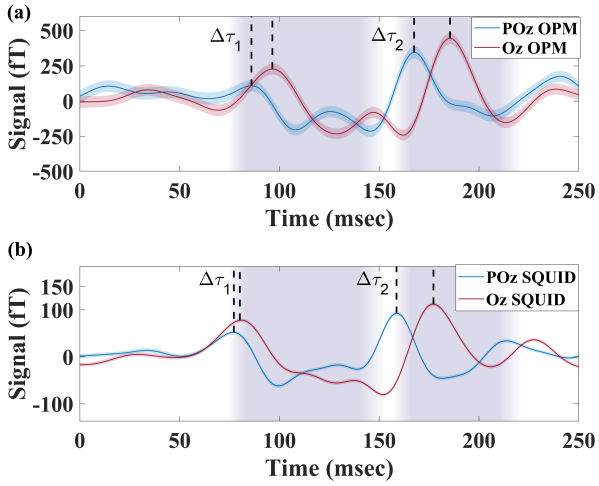

Figure 4: Visually evokes response during flash stimulation recorded by: a) OPM-MEG and b)SQUID-MEG for Participant 1. The coloured areas indicate the limits where the peak onset for Oz is expected for each stimulus. The selected peaks for Oz (red) and POz (blue) sensors are marked with dashed lines for both components P2 and P3.

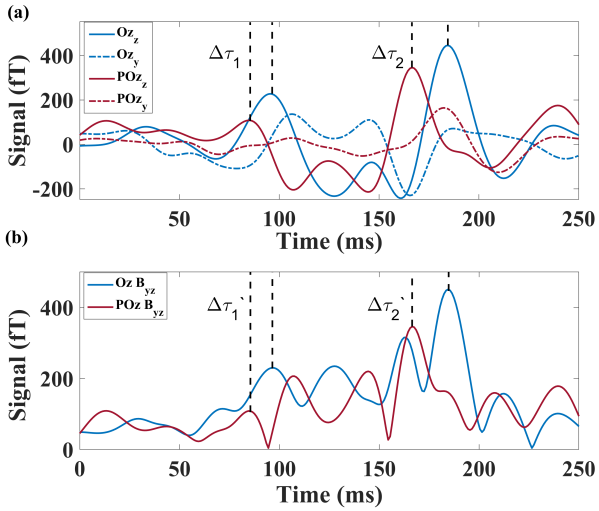

Figure 5: FS VEF recorded at Oz (blue) and POz (red) using OPM-MEG. a) The averaged Oz and POz response along the z (bold) and y (dashed) directions. b) The Oz and POz magnitude projected into the y-z plane. The bold black lines indicate the earlier activation of POz followed by the Oz.

observed across participants and stimuli.

6 DISCUSSION

In this study we use visually evoked brain fields (VEF) to assess and demonstrate the ability of MEG based on two types of highly sensitive magnetometers (OPMs and SQUIDs) to detect neurophysiogical brain signals with simultaneously high spatial and temporal resolution. We find that both sensor modalities are suitable to reproduce characteristic brain signatures known from well-established neurophysiological research and clinical practice.

The ability to track local brain responses in space and time can be quantified by determining the time interval over which a signal rises and falls, i.e. the ratio between the amplitude of a peak signal and the temporal width of the peak. We find that this height to width ratio (HWR) is about fourfold enhanced for OPM measurements over their SQUID counterparts, confirming the expectation of the closer proximity of the OPMs to the visual cortex having such an effect.

Importantly, we were able to confirm that the OPM-MEG measurements are robust. Repeating the experiment with two different visual stimuli (flash stimulus and a checker board pattern reversal stimulus) and with three different participants, we find full reproducibility over multiple repeated runs within each subject and each stimulus. Differences between subjects and type of stimulus are discernable, but the key signal characteristics remain.

Finally, we illustrate that OPM-MEG is able to reliably register neurophysiological signals of a common origin at different locations at different times. This is demonstrated by measuring the arrival times of characteristic VEFs at two distinct locations within the visual cortex. The temporal resolution is sufficiently high to determine significant time differences between the two locations, with a delayed response at the Oz position relative to the POz position on the order of 10-20 ms for the different typical VEF components. This observation is again highly reproducible for different runs and is similar across the participants and the two types of stimuli. It is confirmed by corresponding SQUID measurements. In spite of lower signal to noise levels in our OPM setup, the time delay uncertainties of the OPM data are comparable and even slightly lower than their SQUID counterparts. We attribute this to the strongly enhanced HWR featured by the OPMs.

In order to verify the neuronal nature of the measured time delay, we analysed the recordings along both the OPM's y and z axes. Although we have already demonstrated that our analysis of B_z results in an earlier activation of POz, the inclusion of a second axis, for which we now measure $|B_{yz}|$, follows the same trend. We can indicate that the observed activation pattern is more likely to be from neural activity than an artifact of lim-

ited information. The future addition of a third orthogonal axis, to complement our two axis system, will be required in order to fully validate the activation source observed. As we have demonstrated the reproducibility of VEFs in separate runs, sometimes recorded over subsequent days, acquiring three dimensional recordings by rotating the OPM-MEG sensors between runs could be used in future experiments.

Although the VEF is well defined in humans [39], the spatio-temporal pattern of the propagating signal is not well characterized. Studies have revealed the interaction of the primary visual cortex (V1) with associative visual areas (V2, V3) using an invasive cortical feedback system in animal models [33,34]. The hierarchical order and the spatio-temporal processing of the signal in humans remains uncertain. Some studies have claimed P1 originates from the primary visual cortex [10, 41], while others indicate it originates from the extrastriate cortex [36, 42]. Additionally, the P2/P100 component appears to originate from the extrastriate cortex without a definite region [43]. The widespread sensor positioning of electrodes or SQUIDs combined with the low spatio-temporal resolution may not be able to record coincident responses from close cortical sources. Here, we introduce the OPM-MEG system as a non-invasive investigational tool, with the potential to further detail and explore the structural and functional connectivity of neighbouring cortical areas, with a higher spatio-temporal resolution than currently available. Our initial experiments are consistent with the findings in animal models [33, 34] being applicable also to the human brain.

The benefits of OPM-MEG could be important both at research and clinical levels: its higher spatio-temporal resolution would allow to better investigate neural networks, shedding light on the relationships between the connectivity of functionally related brain areas, along with their frequency synchronization. Moreover, this advancement could be easily applied in clinical populations at different stages, such as those with Alzheimer's disease. In people with mild cognitive symptoms, topographical biomarkers based on the analyses of the frequency domain might monitor the progression of the disease over years and therapy response. However, a higher impact could be achieved especially at a prodromal (or, even better, preclinical) stage, in which these biomarkers could be used as "gatekeepers" for people at risk of developing Alzheimer's disease [44].

In our experiment, the signal noise floor was higher than theoretically possible, leading to a significantly reduced SnR. The electronic noise, the OPM-DAQ settings, or the mounting method of the sensors on the participant's head are among the possible causes. As this study's small sample was limited, future research should aim to demonstrate the reproducibility of our results with a larger population. Moreover, it is important to explore the high spatio-temporal resolution of the OPM-MEG system using different stimuli and explore the propagating signals of different brain circuits. Further research is needed to investigate other sensitive pathways are warranted in order to better establish the suitability of OPM-MEG in its application in neurophysiological studies.

Based on our observations, OPM-MEG could be a reliable neuroimaging method to identify the activation patterns of close cortical regions in response to a specific stimulus. It has the potential to provide a reliable tool for neural speed measurements and the spatio-temporal tracking of propagating signals, including but not limited to further and more detailed investigations of the visual pathway.

DATA AND CODE AVAILABILITY STATEMENT

The raw data and the code used for this paper are available from GitHub (URL to be added).

DECLARATION OF COMPETING INTERESTS

None.

ACKNOWLEDGEMENTS

We gratefully acknowledge insightful discussions with Chris Racey and Jamie Ward. This work was supported by the UK Quantum Technologies Hub for Sensors and Timing (EPSRC grant EP/T001046/1) and by the Core Facility 'Metrology of Ultra-Low Magnetic Fields' at Physikalisch-Technische Bundesanstalt which receives funding from the Deutsche Forschungsgemeinschaft (DFG KO 5321/3-1 and TR 408/11- 1).

References

[1] H. Berger, "Über das Elektrenkephalogramm des Menschen," *Archiv für Psychiatrie und Nervenkrankheiten*, vol. 87, pp. 527–570, 12 1929.

[2] D. Cohen, "Magnetoencephalography: Detection of the Brain's Electrical Activity with a Superconducting Magnetometer," *Science*, vol. 175, pp. 664 LP —- 666, feb 1972.

[3] S. Ogawa, T.-M. Lee, A. S. Nayak, and P. Glynn, "Oxygenation-sensitive contrast in magnetic resonance image of rodent brain at high magnetic fields," *Magnetic Resonance in Medicine*, vol. 14, pp. 68–78, apr 1990.

[4] M. H. Mohajerani, A. W. Chan, M. Mohsenvand, J. LeDue, R. Liu, D. A. McVea, J. D. Boyd, Y. T. Wang, M. Reimers, and T. H. Murphy, "Spontaneous cortical activity alternates between motifs defined by regional axonal projections," *Nature neuroscience*, vol. 16, pp. 1426–1435, oct 2013.

[5] J. Fiser, C. Chiu, and M. Weliky, "Small modulation of ongoing cortical dynamics by sensory input during natural vision," *Nature*, vol. 431, no. 7008, pp. 573–578, 2004.

[6] R. M. Chapman, M. N. Gardner, R. Klorman, M. Mapstone, A. P. Porsteinsson, I. M. Antonsdottir, and L. Kamalyan, "Temporospatial components of brain ERPs as biomarkers for Alzheimer's disease," *Alzheimer's & dementia (Amsterdam, Netherlands)*, vol. 10, pp. 604–614, aug 2018.

[7] M. Song, M. Kang, H. Lee, Y. Jeong, and S. B. Paik, "Classification of Spatiotemporal Neural Activity Patterns in Brain Imaging Data," *Scientific Reports*, vol. 8, no. 1, pp. 1–12, 2018.

[8] F. Di Lorenzo, C. Motta, E. P. Casula, S. Bonnì, M. Assogna, C. Caltagirone, A. Martorana, and G. Koch, "LTP-like cortical plasticity predicts conversion to dementia in patients with memory impairment," *Brain Stimulation*, vol. 13, no. 5, pp. 1175–1182, 2020.

[9] U. B. Barnikol, K. Amunts, J. Dammers, H. Mohlberg, T. Fieseler, A. Malikovic, K. Zilles, M. Niedeggen, and P. A. Tass, "Pattern reversal visual evoked responses of V1/V2 and V5/MT as revealed by MEG combined with probabilistic cytoarchitectonic maps," *NeuroImage*, vol. 31, no. 1, pp. 86–108, 2006.

[10] F. Di Russo, A. Martínez, M. I. Sereno, S. Pitzalis, and S. A. Hillyard, "Cortical sources of the early components of the visual evoked potential," *Human Brain Mapping*, vol. 15, no. 2, pp. 95–111, 2002.

[11] W. Orrison and J. Lewine, *Functional Brain Imaging*, vol. 52. Mosby, 1995.

[12] C. Babiloni, V. Pizzella, C. D. Gratta, A. Ferretti, and G. L. Romani, "Chapter 5 Fundamentals of Electroencefalography, Magnetoencefalography, and Functional Magnetic Resonance Imaging," *International Review of Neurobiology*, vol. 86, no. 09, pp. 67–80, 2009.

[13] P. K. Mandal, A. Banerjee, M. Tripathi, and A. Sharma, "A Comprehensive Review of Magnetoencephalography (MEG) Studies for Brain Functionality in Healthy Aging and Alzheimer's Disease (AD)," *Frontiers in Computational Neuroscience*, vol. 12, pp. 1–40, 2018.

[14] K. T. E. Olde Dubbelink, A. Hillebrand, D. Stoffers, J. B. Deijen, J. W. R. Twisk, C. J. Stam, and H. W. Berendse, "Disrupted brain network topology in Parkinson's disease: A longitudinal magnetoencephalography study," *Brain*, vol. 137, no. 1, pp. 197–207, 2014.

[15] K. Barik, K. Watanabe, J. Bhattacharya, and G. Saha, "Classification of Autism in Young Children by Phase Angle Clustering in Magnetoencephalogram Signals," *2020 National Conference on Communications (NCC)*, pp. 1–6, 2020.

[16] B. T. Dunkley, R. Jetly, E. W. Pang, and M. J. Taylor, "New perspectives on the neurobiology of PTSD: High-resolution imaging of neural circuit (dys)function with magnetoencephalography," *Journal of Military, Veteran and Family Health*, vol. 6, no. S1, pp. 16–25, 2020.

[17] S. Baillet, "Magnetoencephalography for brain electrophysiology and imaging," *Nature Neuroscience*, vol. 20, no. 3, pp. 327–339, 2017.

[18] N. Coquelet, X. De Tiège, F. Destoky, L. Roshchupkina, M. Bourguignon, S. Goldman, P. Peigneux, and V. Wens, "Comparing MEG and high-density EEG for intrinsic functional connectivity mapping," *NeuroImage*, vol. 210, p. 116556, 2020.

[19] J. Gross, S. Baillet, G. R. Barnes, R. N. Henson, A. Hillebrand, O. Jensen, K. Jerbi, V. Litvak, B. Maess, R. Oostenveld, L. Parkkonen, J. R. Taylor, V. Van Wassenhove, M. Wibral, and J.-M. Schoffelen, "Comments and Controversies Good practice for conducting and reporting MEG research," *NeuroImage*, vol. 65, pp. 349–363, 2013.

[20] J. C. Allred, R. N. Lyman, T. W. Kornack, and M. V. Romalis, "High-Sensitivity Atomic Magnetometer Unaffected by Spin-Exchange Relaxation," *Physical Review Letters*, vol. 89, p. 130801, sep 2002.

[21] C.-H. Lin, T. M. Tierney, N. Holmes, E. Boto, J. Leggett, S. Bestmann, R. Bowtell, M. J. Brookes, R. C. Miall, and G. R. Barnes, "Using optically-pumped magnetometers to measure magnetoencephalographic signals in the human cerebellum," *bioRxiv*, p. doi.org/10.1101/425447, 2018.

[22] E. Boto, R. Bowtell, P. Krüger, T. M. Fromhold, P. G. Morris, S. S. Meyer, G. R. Barnes, and M. J. Brookes, "On the potential of a new generation of magnetometers for MEG: A beamformer simulation study," *PLoS ONE*, vol. 11, no. 8, pp. 1–16, 2016.

[23] S. Tan, B. J. Roth, and J. P. Wikswo, "The magnetic field of cortical current sources: the application of a spatial filtering model to the forward

and inverse problems," *Electroencephalography and Clinical Neurophysiology*, vol. 76, no. 1, pp. 73–85, 1990.

[24] E. Boto, S. S. Meyer, V. Shah, O. Alem, S. Knappe, P. Kruger, T. M. Fromhold, M. Lim, P. M. Glover, P. G. Morris, R. Bowtell, G. R. Barnes, and M. J. Brookes, "A new generation of magnetoencephalography: Room temperature measurements using optically-pumped magnetometers," *NeuroImage*, vol. 149, no. January, pp. 404–414, 2017.

[25] J. Iivanainen, M. Stenroos, and L. Parkkonen, "Measuring MEG closer to the brain: Performance of on-scalp sensor arrays," *NeuroImage*, vol. 147, pp. 542–553, 2017.

[26] B. Hochwald and A. Nehorai, "Magnetoencephalography with diversely oriented and multicomponent sensors," *IEEE Transactions on Biomedical Engineering*, vol. 44, no. 1, pp. 40–50, 1997.

[27] S. Jbabdi, S. N. Sotiropoulos, A. M. Savio, M. Graña, and T. E. J. Behrens, "Model-based analysis of multishell diffusion MR data for tractography: how to get over fitting problems," *Magnetic resonance in medicine*, vol. 68, pp. 1846–1855, dec 2012.

[28] S. Warrington, K. L. Bryant, A. A. Khrapitchev, J. Sallet, M. Charquero-Ballester, G. Douaud, S. Jbabdi, R. B. Mars, and S. N. Sotiropoulos, "XTRACT - Standardised protocols for automated tractography in the human and macaque brain," *NeuroImage*, vol. 217, p. 116923, 2020.

[29] T. Sander, A. Jodko-Władzińska, S. Hartwig, R. Brühl, and T. Middelmann, "Optically pumped magnetometers enable a new level of biomagnetic measurements," 2020.

[30] S. Knappe, T. Sander, and L. Trahms, "Optically-Pumped Magnetometers for MEG," in *Magnetoencephalography From Signals to Dynamic Cortical Networks*, vol. 9783642330, ch. Part VI, pp. 993–999, Springer, Berlin, Heidelberg, 2014.

[31] J. V. Odom, M. Bach, M. Brigell, G. E. Holder, D. L. McCulloch, A. Mizota, and A. P. Tormene, "ISCEV standard for clinical visual evoked potentials: (2016 update)," *Documenta Ophthalmologica*, vol. 133, no. 1, pp. 1–9, 2016.

[32] R. Oostenveld and P. Praamstra, "The five percent electrode system for high-resolution EEG and ERP measurements," *Clinical Neurophysiology*, vol. 112, no. 4, pp. 713–719, 2001.

[33] P. E. Roland, A. Hanazawa, C. Undeman, D. Eriksson, T. Tompa, H. Nakamura, S. Valentiniene, and B. Ahmed, "Cortical feedback depolarization waves: A mechanism of top-down influence on early visual areas," *Proceedings of the National Academy of Sciences of the United States of America*, vol. 103, no. 33, pp. 12586–12591, 2006.

[34] W. Xu, X. Huang, K. Takagaki, and J.-y. Wu, "Compression and Reflection of Visually Evoked Cortical Waves," *Neuron*, vol. 55, no. 1, pp. 119–129, 2007.

[35] R. Oostenveld, P. Fries, E. Maris, and J.-M. Schoffelen, "FieldTrip: Open Source Software for Advanced Analysis of MEG, EEG, and Invasive Electrophysiological Data," *Computational Intelligence and Neuroscience*, vol. 2011, p. 156869, 2011.

[36] J. J. Foxe, E. C. Strugstad, P. Sehatpour, S. Molholm, W. Pasieka, C. E. Schroeder, and M. E. McCourt, "Parvocellular and magnocellular contributions to the initial generators of the visual evoked potential: High-density electrical mapping of the "C1" component," *Brain Topography*, vol. 21, no. 1, pp. 11–21, 2008.

[37] H. Pratt, N. Bleich, and W. H. Martin, "Short latency visual evoked potentials to flashes from light-emitting diodes," *Electroencephalography and Clinical Neurophysiology/ Evoked Potentials*, vol. 96, no. 6, pp. 502–508, 1995.

[38] R. Sharma, S. Joshi, K. D. Singh, and A. Kumar, "Visual evoked potentials: Normative values and gender differences," *Journal of Clinical and Diagnostic Research*, vol. 9, no. 7, pp. 12–15, 2015.

[39] D. A. Jeffreys and J. G. Axford, "Source locations of pattern-specific components of human visual evoked potentials. I. Component of striate cortical origin," *Experimental Brain Research*, vol. 16, no. 1, pp. 1–21, 1972.

[40] K. L. Coburn, R. T. Amoss, J. E. Arruda, L. D. Kizer, and Y. S. Marshall, "Effects of flash mode and intensity on P2 component latency and amplitude," *International Journal of Psychophysiology*, vol. 55, no. 3, pp. 323–331, 2005.

[41] S. Vanni, T. Tanskanen, M. Seppä, K. Uutela, and R. Hari, "Coinciding early activation of the human primary visual cortex and anteromedial cuneus," *Proceedings of the National Academy of Sciences*, vol. 98, pp. 2776 LP —- 2780, feb 2001.

[42] F. Yoshida, M. Hirata, A. Onodera, T. Goto, H. Sugata, and S. Yorifuji, "Noninvasive spatiotemporal imaging of neural transmission in the subcortical visual pathway," *Scientific Reports*, vol. 7, no. 1, pp. 1–6, 2017.

[43] F. Di Russo, A. Martínez, M. I. Sereno, S. Pitzalis, and S. A. Hillyard, "Cortical sources of the early components of the visual evoked potential," *Human Brain Mapping*, vol. 15, no. 2, pp. 95–111, 2002.

[44] C. Babiloni, K. Blinowska, L. Bonanni, A. Cichocki, W. De Haan, C. Del Percio, B. Dubois, J. Escudero, A. Fernández, G. Frisoni, B. Guntekin, M. Hajos, H. Hampel, E. Ifeachor, K. Kilborn, S. Kumar, K. Johnsen, M. Johannsson, J. Jeong, F. LeBeau, R. Lizio, F. Lopes da Silva, F. Maestú, W. J. McGeown, I. McKeith, D. V. Moretti, F. Nobili, J. Olichney, M. Onofrj, J. J. Palop, M. Rowan, F. Stocchi, Z. M. Struzik, H. Tanila, S. Teipel, J. P. Taylor, M. Weiergräber, G. Yener, T. Young-Pearse, W. H. Drinkenburg, and F. Randall, "What electrophysiology tells us about Alzheimer's disease: a window into the synchronization and connectivity of brain neurons.," *Neurobiology of aging*, vol. 85, pp. 58–73, jan 2020.